Prediction Of The Influence Of Cutting Conditions On Surface Morphology After Its Thermal Spraying With Stellite 6 Alloy

Jan Řehoř
University of West Bohemia
Miroslav Gombár
University of West Bohemia
Marta Harničárová (marta.harnicarova@gmail.com)
University of West Bohemia https://orcid.org/0000-0002-8384-721X
Milena Kušnerová
University of West Bohemia
Šárka Houdková-Šimůnková
University of West Bohemia
Jan Valíček
University of West Bohemia
Jaroslava Fulemová
University of West Bohemia
Alena Vagaská
University of West Bohemia

Research Article

Keywords: coatings, hot spray, Stellite 6, longitudinal turning, surface roughness

Posted Date: February 15th, 2022

DOI: https://doi.org/10.21203/rs.3.rs-1336218/v1

Abstract

The presented paper is devoted to the basic influences of the cutting conditions on the basic parameters of the roughness of the surface machined by longitudinal turning; the investigated surface was before the machining modified by the technology of thermal spraying. High-speed Oxy-Fuel (HVOF) thermal sprays, in particular, Stellite 6 sprays based on Cobalt and Chromium alloy, are widely used in the industry thanks to their excellent mechanical properties, wear resistance, corrosion resistance and good temperature stability in comparison with steel for example. From experimental results in the specified range of cutting speeds, feeds and cutting depths, new predictive models of roughness parameters were compiled using mathematical and statistical methods, followed by application of neural networks in order to confirm the obtained conclusions. Research results have proved that feed turning technology is a suitable technology for machining coatings generated by Stellite 6 alloy thermal sprays in such user cases where additional surface treatment is required for specific reasons.

1 Introduction

Cobalt and Chromium alloys are considered to be a very attractive material for applications in many technical fields; coatings prepared with thermal spraying technologies are used in virtually every industrial sector that specifies requirements for their service life and quality, such as aviation industry, mechanical engineering, biomedical engineering, nuclear technology and production of tur- bines [1–2]. Their wide use is attributed mainly to excellent properties, such as wear resistance, corrosion resistance, high-temperature resistance and resistance to electric puncture, and they have also very good bio-compatibility [3–6]. Friction and corrosion resistant coatings are applied on shafts on their functional surfaces under bearings, crankshafts, helices, piston rods, at the entering edges of ploughs or blades of water turbines. Coatings resistant to high temperature are applied to blades of aeroplane or power turbines and combustion chambers. Coatings resistant to electric punctures are used for bearings, pulleys and contacts of heavy-current circuit breakers. Coatings of cobalt chrome are used in biomedical applications, especially in dental implants or orthopaedic replacements [7], especially in implants of heavily loaded joints, such as knee and hip joint [8–9].

Cobalt-based alloys were first introduced by E. Hayes as hard metals resistant to all types of wear and corrosion, as well as to high-temperature oxidation. This material is now known as the Stellite alloy invented by the American company Elwood Hayness at the beginning of the last century. This cobalt-based alloy is based on cobalt as the main component, but it may contain a significant amount of nickel, chromium, tungsten, small amounts of molybdenum, niobium, tantalum, titanium, lanthanum and other alloying elements [10]. For example, the presence of molybdenum in the composition of cobalt alloys refines grain size, thereby increasing solidification of the solid solution with subsequent improvement of the mechanical properties of these alloys [11]. The material may be manufactured and used in technical practice in a variety of ways such as wire, powder for hard surfaces, thermal spraying, spray welding and other desired processes specifically in dependence on the composition of the Stellite alloy.

An increase in the mechanical strength of the primary structure of the cobalt base alloy depends primarily on its material composition, on the form of carbide in the cobalt matrix, and on the grain boundaries. The alloys Co- Cr-Mo (F75), are usually produced by casting, the alloys Co-Cr-W-Ni (F90), Co-Ni-Cr-Mo (F562), Co-Ni-Cr-Mo-W-Fe (F563) are produced by forming and forging [12]. No less important contribution to the increase in the mechanical strength of cobalt-based alloys is their coating with the use of High-Velocity Oxy-Fuel (HVOF) technology.

At present, new solutions for surface treatments and hard protective coatings are being investigated in order to improve the properties of materials used in the most demanding applications [13]. An example of the demanding applications of surface treatments is the work of the authors [14] who have reported the use of erosion-resistant coatings, such as particularly CrN, TiN, TiAlN and TiSiN in the engine components in the aviation industry. Hard chrome coatings for wear-resistant applications in the automotive industry are also known [15]. Increase in the number and importance of applications of thermal spraying processes makes it possible to replace the traditional applications of hard chromium by thermal spraying, e.g. for electrodes [16]. The WC-Co cermets are one of the main hard materials used for the production of coatings; the cermets are specifically used for thermal spraying [17]. The main properties of WC-Co coatings include requirements for hardness and wear resistance [18]. At present some other cobalt-based Stellite alloys are also available that offer excellent wear resistance, high heat resistance and high corrosion resistance [19–20].

In most applications, the use of coatings requires a guarantee of an adequate quality even a long time after the manufacture. As a result, conventional machining processes are introduced for an effective finish of the coatings. Machining of such coatings is extremely difficult precisely because these alloys retain their strength and hardness even at elevated temperatures generated by the machining process. Low thermal conductivity, high hardness at elevated temperature and high wear resistance are the cause of the very difficult processability of cobalt, chromium and molybdenum alloys.

High attention is paid to conventional operations, such as turning, compared to conventional used grinding technology, in order to reduce machining times. Hard turning is considered to be an adequate method of substitution of grinding when machining high hardness materials [21]. In machining processes, however, the high hardness of the coatings often results in high cutting forces and cutting temperatures, and it consequently decreases the tool service life [22]. The relationship between hardness and wear of the tool was experimentally analysed by the authors [23], and it was found that increasing the hardness of the steel from 35 to 45 HRC increases wear of the cutting edge. Increased attention should also be paid to the process of production of the coating as such. For example, coatings formed by application of thermal spraying are anisotropic, which affects several properties: hardness, modulus of elasticity and fracture toughness [24]. According to the authors [25], the machining of coatings, especially after thermal spraying, has to address two main problems: the adhesion of the coating to the substrate and the wear of the tool.

Moreover, the authors [26] state that the efficiency of the machining process depends on the structure and properties of the materials in contact. The expected and desirable results, therefore, depend to a large extent on selected tool materials and selected machining parameters [27]. An adequate selection of machining parameters can help to achieve acceptable surface quality and tool wear. Typically, cutting rates of approx. 30 - 40 m·min −1 and relatively low values of cutting depth and feed rate are used [25]. Although machining is a complex process that is influenced by many factors, the current studies focus on selecting the machining parameters for turning operations. An empirical and mechanical approach to selecting machining parameters is identified by the authors [28] for surface roughness analysis, although both approaches could be used for assessment of other outputs. The considerable complexity of the mechanical approach is simplified by the empirical approach, that's why usually several experimental tests with different machining parameters are usually performed to predict the final effect on the results. The empirical methodology is particularly suitable for machining processes, which represent a strong background for stabilising the initial values of the machining parameters. However, this background is not large enough for machining of coatings, cutting of which is difficult. Although the choice of machining parameters plays an important role in the process results, it should be emphasized that other factors can also have a significant impact. For example, the authors [29] identified the tool vibrations, the appearance of ruptures, adhesion, material deposits, elastic and plastic deformations and tool wear as basic factors for achieving surface quality. The influence of machining parameters is more accepted in the scientific literature than it is monitored by technical practice; in this sense, more results of the machining process are affected. In the case of hard turning, the authors [30] confirmed the influence of cutting rate, cutting depth, feed rate and machining times, surface roughness and wear of the tool. The effects of machining parameters on the surface quality are given by the authors [31], who evaluated the turning of sintered WC-25Co with the use of cutting tools by the tests, which identified an unequivocal relationship between cutting rate and surface roughness. At cutting rates of 15 and 40 m·min −1 the surface roughness was limited to less than 0.2 μm for all machining times tested. However, at a cutting rate of 100 m·min −1, the surface roughness achieved significantly higher values and reduced the machining time.

On the other hand, the authors [32] found that the choice of feed rate (from 0.03 to 0.3 mm·rev −1) played an important role in the development of surface roughness. When analyzing the effect of cutting depth, it was found that the use of sharp tools caused an increase in cutting depth and lower values of surface roughness. The authors [33] evaluated the influence of cutting rate and feed rate on the surface roughness by turning Stellite 6 using tungsten carbide and ceramic-reinforced ceramic tools. They found a great influence of the feed rate on the surface roughness value, but the effect of cutting rate was lower. Test tested feed rates ranged from 0.1 to 0.2 mm·rev −1 for tungsten carbide tools and from 0.25 to 0.35 mm·rev −1 for fibre-reinforced ceramic; the cutting rate was set from 30 to 50 m·min −1 (for tungsten carbides) and from 30 to 90 m·min −1 (for ceramics). The optimal surface roughness was achieved by using low feed rates and high cutting rates.

It means that the hardness of Stellite coatings is the main factor that makes the machining process more difficult. Based on published findings, the authors of this paper ask the key question as to how efficient

and effective is machining of Stellite 6 coatings in current technical practice.

2 Methods

The Co-Cr-W Stellite 6 alloy, which is most widely used in industrial applications, was used for the presented experiments. Its exceptional wear resistance is mainly due to the unique properties of the hard carbide phases dispersed in the CoCr matrix. Various coating technologies, such as plasma transfer arc (PTA), inert tungsten gas (TIG) welding, thermal spraying or laser coating, can be used to deposit the Stellite layer on the surface. The chemical composition of the Stellite 6 spray obtained from the scanning electron microscopy/energy dispersive X-ray spectroscopy (SEM/EDX, Carl Zeiss s.r.o., Prague, Czech Republic) measurements [34], with the density of the test material being 8.44 g cm^{-3}.

[Table 1 about here.]

Table 1 Nominal composition (mass %) and basic physical properties of the Stellite 6 coating

	Co	Cr	W	Mo	Si	Mn	Ni	Fe	C
Wt. %	59.56	25.35	4.02	1.66	1.40	0.33	1.67	0.87	2.14

Thermal spraying is an advanced technology for depositing thick coatings (50- 500 μm), its principle is illustrated in Figure 1. The coating material is usually delivered as small particles to a spray device where it is heated and accelerated towards the surface of the substrate. The molten particles gradually touch the surface of the substrate, where they deform into scales and lamellae in the form of a disc and then quickly solidify. Repeated impact of particles creates a coating with a typical lamellar microstructure and with specific anisotropic properties [34].

[Table 2 about here.]

Table 2 Nominal values of stresses at room temperature of the Stellite 6coating

	Rm	Rp(0.2)	elongation	Young's modulus of elasticity
Stellite 6	1265 MPa	750 MPA	3-5 %	237 GPa

Thermal spraying is an advanced technology for depositing thick coatings (50- 500 μm), coating material is usually delivered as small particles to a spray device where it is heated and accelerated towards the surface of the substrate. The molten particles gradually touch the surface of the substrate, where they deform into scales and lamellae in the form of a disc and then quickly solidify. Repeated impact of particles creates a coating with a typical lamellar microstructure and with specific anisotropic properties [34].

In addition to deformed particles, the microstructure of the coating applied by thermal spraying also contains numerous defects, such as oxides, pores and impurities. Oxides originate in particular from the oxidation of the surface of the particles formed during the process of spraying. Porosity and unprocessed particles are formed as a result of non-optimal heating and acceleration of flying particles and their improper propagation after impact. The presence of defects naturally reduces the mechanical properties of the coating, such as hardness, strength in cohesion, toughness and consequently also functional properties, such as wear resistance [35]. The nature of the coating defects determines its quality [34].

Although different techniques of thermal spraying were developed (e.g. plasma spraying, flame spraying, cold spraying, etc.) used for different types of coating materials in connection with various applications, the HVOF technology for spraying metal and hard metal is the most suitable. High speed combined with medium temperatures reduces the amount of oxidation of particles' surface during the spraying process and allows the formation of coatings with low porosity and small amounts of internal oxides [34, 35].

The HP/HVOF JP500 spraying technology was used for the realisation of the presented experiments at the Research and Testing Institute in Pilsen, Ltd. The parameters of spraying are summarised in Table 3. The condition before spraying with alumina was the following: grain size 0.8-1 mm (F22); roughness *Ra* = 8 μm; component FST 484.074 Stellite 6; alloy based on powdered alloy, with a nominal composition of 28% Cr; 5% W; 1.2% C; 1% Si. Atomised particles of 20-53 μm were used for spraying.

[Table 3 about here.]

Table 3 Spraying parameters.

Parameter	Value
Oxygen	996 l×min^{-1}
Fuel	277 l×h^{-1}
Barrel length	150 mm
Spray distance	360 mm
Traverse speed	250 mm×s^{-1}
Feed rate	46 g×min^{-1}
Carrier gas	Nitrogen, 6.5 l×min^{-1}
Offset	6
Number of passes	7

It is evident from the SEM microstructure that the amount of porosity is low without the occurrence of any cracks or deformations. At larger magnification, the gap between the splask and the inner dendritic microstructure can be seen. Using the HVOF technology, the Stellite 6 coating microstructure, consisting of two cohesive Co-based solids, the main cover centre (fcc) and the less dominant hexagonal tightly closed (hcp), was applied by spraying. At a mechanical load, the fcc Co tends to convert to hcp-Co. The pressure-induced martensitic transformation that is responsible for hardening is one of the main sources of low wear and high erosion resistance of cobalt-based alloys. Transformation mechanisms of pure cobalt and its alloys were described in various studies [35]. Unlike cast Stellite 6 or in the form of laser-applied microscopic paint, HVOF does not contain carbide particles due to the high speed of solidification at spraying. The microstructure of the test coating is analysed in more detail in the works [35]. Several experiments were carried out as part of experimental verification. For the first experiment,

cylindrical specimens of 54.7 mm in diameter from the C45 base material were used, on which a Stellite 6 was applied by thermal spraying with an average value of 0.55 mm. The thickness of the machined layer was set to 88 mm. The tool TUNGALOY RNGN 120400 LX11 43 was used, which was clamped in the tool holder MRGNR2525M12. The experiments were verified on the MASTURN 50/C80 engine centre lathe according to the conditions outlined (Table 4). A view of the experiment is shown in Figure 1.

[Fig. 1 about here.]

[Table 4 about here.]

Table 4 Conditions of experimental verification (experiment 1).

TEST	TOOL	v_c	f_{rev}	a_p	Machining length
		$m \times min^{-1}$	$mm \times rev^{-1}$	mm	mm
1	RNGN43-LX11-TUNGALOY	150	1	0.15	20
2	RNGN43-LX11-TUNGALOY	150	1	0.15	20
3	RNGN43-LX11-TUNGALOY	150	1	0.15	20
4	RNGN43-LX11-TUNGALOY	150	1	0.15	20
5	RNGN43-LX11-TUNGALOY	150	0.6	0.1	15
6	RNGN43-LX11-TUNGALOY	150	0.6	0.1	15
7	RNGN43-LX11-TUNGALOY	150	0.6	0.1	15
8	RNGN43-LX11-TUNGALOY	150	0.6	0.1	15
9	RNGN43-LX11-TUNGALOY	150	0.4	0.1	15
10	RNGN43-LX11-TUNGALOY	150	0.4	0.1	15
11	RNGN43-LX11-TUNGALOY	150	0.4	0.1	15
12	RNGN43-LX11-TUNGALOY	150	0.4	0.1	15
13	RNGN43-LX11-TUNGALOY	250	0.4	0.1	15
14	RNGN43-LX11-TUNGALOY	250	0.4	0.1	15
15	RNGN43-LX11-TUNGALOY	250	0.4	0.1	15
16	RNGN43-LX11-TUNGALOY	250	0.4	0.1	15

The morphology of the machined area was monitored by the contact profile meter HOMMEL-ETAMIC TURBO WAVE V7.45 with the following settings:

- sensor - TKU300;
- measuring range - 80 μm;
- measuring track l_t - 4.80 mm;
- feed rate v_t - 0.50 mm·s^{-1}.

The following parameters of surface roughness were selected as the basic indicators of the morphology of the machined surfaces as part of the experimental verification:

- arithmetical centre of absolute deviations of the filtered roughness profile from the centre line within the basic measuring length l_r - *Ra*;
- medium depth of roughness, i.e., the average value calculated from 5 values of *Rz* and 6 values of basic lengths l_r.

For experiment 2, instruments with positive geometry were chosen, namely circular plates made of cermet marked as:

- RCHT 12 04MO-PL 530;
- RCKT 12 04MO-WM 530.

For these plates, a clamp C5-SRDCN00060-12AHPA was selected, which was fixed using the CAPTO C5 onto the dynamometer (Spike by Promicron), and the dynamometer was then clamped to the milling spindle. A plan of the experiment was drawn up, according to which the selected plates were tested at a cutting rate of 320 and 80 mm·min-1and at a feed rate of 0.3 mm·rev^{-1}. In both cases, the cutting blades were quickly destroyed due to the considerable positive geometry of the tool (γ = 20 °). The experiments were performed on a tooling machine DMG MORI CTX BETA 1250. Experimental data of surface roughness parameters were processed by mathematical-statistical methods, and the results were interpreted [36].

3 Results And Discussion

3.1. Results and discussion for parameter Ra

From the viewpoint of the chip machining of the coating after it's spraying with the alloy Stellite 6, two specific problems arose that caused worse machinability. From the viewpoint of machinability, it was mainly the boundaries of the splat, which did not concern the grain boundaries but the boundaries of the deformed particles. Cohesiveness between splats is lower, particularly for Stellite 6. The splat boundaries can be formed by the oxides formed during the flame particle flight during flame annealing. The second problem was the alloy material as such. The Stellite within the splat undergoes a deformation induced martensite transformation from the fcc to the hcp grid. During machining, it hardens and becomes brittle, similarly as some types of steel. The behaviour of the investigated objects can generally be described using models that can explain the logical relationships of objects, but sometimes

they must do with finding a mathematical function that determines the dependence between factors and responses for the objects in question, although it is impossible to answer unequivocally why is it so. The monitored responses in the presented experiment can be searched and verified using a mathematical model using statistical tools. This method makes it possible to describe how the given response depends on individual factors. Due to the fact that, in the case of surface roughness profile parameters the attention was paid mainly to the basic parameters of roughness *Ra*, *Rz*, two models were sought for these two responses. For the *Ra* parameter, the model is formulated in (1) as a relation with variables v_c cutting rate, f_{rev} feed rate and a_P depth of cut.

$$Ra = const \cdot v_c^{x_1} \cdot f_{rev}^{x_2} \cdot a_P^{x_3} \quad (1)$$

The analysis shows that the model (1) with the action of the constant tool RNGN43 LX11 TUNGALOY accounts for 99.81% of the variability of the investigated parameter *Ra*. This conclusion can be accepted on the basis of the value of the adjusted index of determination. The mean value of *Ra* = 1.98 μm and estimation of the standard deviation of random error is 0.051968. The chosen mathematical and statistical dependence according to the Cohen scale can, therefore, be considered as functional. Furthermore, the adequacy of the selected model was tested using analysis of variance (Table 5) by testing the zero-statistic hypothesis H_0, which resulted from the nature of the test and provided information that none of the effects used in the model affected the significant change of the investigated variable. It followed from the subject test that the achieved level of significance (Prob> F) was less than the chosen significance level α = 0.05 and that it could be concluded that there was not enough evidence for accepting the H_0 hypothesis, i.e. that it could be stated that the model (1) was significant. It also follows that part of the total variability of the experimentally obtained values, which corresponds to random errors, is significantly smaller than the variability of the measured values in accordance with the model.

[Table 5 about here.]

Table 5 Analysis of variance by testing the zero statistic hypothesis H_0.

Source	DF	Sum of Squares	Mean Square	F Ratio	Prob > F
Model	3	1.2680028	0.422668	2710.275	<0.0001
Error	12	0.0018714	0.000156		
C. Total	15	1.2698742			

On the basis of testing of the adequacy of the used statistical model lzr it is possible to determine the regression coefficients of statistical dependence defined in (1) using the smallest square method (Table 6).

[Table 6 about here.]

Table 6 Estimates of the parameter of the investigated dependence for the variable *Ra*.

Term	Estimate	Std Error	t Ratio	Prob>|t|	Lower 95 %	Upper 95%
Const	-1.7870540	0.137774	-12.97	<0.0001*	-2.0872390	-1.4868700
x_1	0.5748062	0.039803	14.44	<0.0001*	0.4880820	0.6615305
x_2	2.4733928	0.050146	49.32	<0.0001*	2.3641331	2.5826525
x_3	-1.4709540	0.098357	-14.96	<0.0001*	-1.6852560	-1.2566530

* - significant at the significance level $\alpha = 0.05$.

After substitution of the values of the individual regression coefficients (Table 6) calculated by the least squares method into the general form of the model (1) we get the final form of the dependence (2) for further analysis of the dependence of *Ra* value on the cutting conditions.

$$Ra = 0.016 \cdot v_c^{0.575} \cdot f_{rev}^{2.473} \cdot a_p^{-1.471} \qquad (2)$$

An analysis of the influence of the individual investigated input variables on the change of the *Ra* value is shown in Figures 2 and 3. It is obvious that with an increase in the cutting speed the value of the mean arithmetic deviation of the roughness profile also increases. Figure 2 illustrates an experimentally obtained model describing the given relationship for constant parameters: constant feed rate, constant cutting depth, and constant machining length, due to the influence of the given input factors on the change of the *Ra* value. The influence of the cutting rate on the change of observed response *Ra* is 15.75%. Given the validity of the predictive model (1) at the selected range of the cutting rate from 150 to 250 m·min^{-1}, it can be stated that within the given interval an increase of the cutting rate by 10 m·min^{-1} will cause an increase of the *Ra* value by 0.027 μm, with fulfilment of other conditions ensuing from the nature of mathematical and statistical modelling. The validity of the model (1) is limited to the interval of the used cutting conditions, and the validity beyond of those intervals has to be always verified experimentally.

[Fig. 2 about here.]

The feed rate f_{rev} as the second investigated input factor has a 53.79 % influence on the change in the value of the observed response of the surface roughness *Ra*. It may be stated that with an increase in the feed value the value of the mean arithmetic deviation of the roughness profile increases as well. The influence of feed rate on the roughness of the machined surface results from the kinematics of the

machining technology. From the machining theory, it is obvious that with the increase in feed rate the corrugation of the machined surface increases. Research performed by many authors shows that, at higher feed rates, the cutting rates have a smaller influence on the quantitative values describing the micro-geometry of the machined surface. These conclusions are also documented by the results of this experiment (Figure 3).

[Fig. 3 about here.]

More profound analysis of the statistically most significant factor - the feed rate frev on the change of the observed response *Ra*, shows that the conditional value *Ra* (Figure 3) also increases within the range of the experimentally used values of feed rate with its increase. Since the feed rate plays a major role in changing the Ra value, its influence can be further analysed by the Kruskal-Wallis nonparametric test (Table 7). The Kruskal-Wallis analysis of variance tests the zero hypothesis, i.e. that all mean values in the investigated groups, in this case in the individual levels of experimentally used feed rates, are the same. On the basis of the achieved level of significance of the Kruskal-Wallis test (p = 0.017), it can be concluded that at the chosen level of significance α = 5 % a statistically significant difference in the value of the mean arithmetic variance of the roughness profile *Ra* based on the change of the feed rate value was proven. This conclusion can be naturally accepted only on the basis of an assumption that the cutting rate and the depth of cut do not affect the change of the *Ra* value. However, since their impact is within the interval of 15.75 % for the cutting rate and 16.32 % for the cutting depth, this assumption can be accepted for the discussed need.

[Table 7 about here.]

Table 7 Results of the Kruskal-Wallis test of difference of the *Ra* value in dependence on the change of the feed rate.

Depend. *Ra* [µm]	Kruskal-Wallis ANOVA by Ranks; *Ra* [µm] Independent (grouping) variable: f_{rev} [mm·rev^{-1}] Kruskal-Wallis test: H(2, N=16)=12.72459; *p*=0.0017			
	Code	Valid N	Sum of Ranks	Mean Rank
0.4 mm·rev^{-1}	101	8	36.00000	4.50000
0.6 mm·rev^{-1}	102	4	42.00000	10.50000
1.0 mm·rev^{-1}	103	4	58.00000	14.50000

It is necessary to realise in this context that the Kruskal-Wallis test does not work with the original values but with the sequential numbers that were assigned. From the values of the sum of the order (Figure 8), it can be seen that the lowest values of the observed response *Ra* were achieved at the feed rate of 0.4 mm/hr^{-1} and with the continuous increase of the feed rate value the *Ra* values also increased. The results are consistent with the previous conclusions. When comparing the achieved levels of significance p (Table 8), it can be seen that the statistically significant difference in the achieved *Ra* value is only between the feed rate of 0.4 mm·rev^{-1} and 1.0 mm·rev^{-1}. The difference of the observed response *Ra*

between the mm·rev^{-1} and 0.6 mm·rev^{-1}, as well as between 0.6 mm·rev^{-1} and 1.0 mm·rev^{-1} was not proven.

[Table 8 about here.]

Table 8 Multiple comparisons of the *p*-values of the differences of *Ra* depending on the change in the feed rate f_{rev}.

Dependent *Ra* [µm]	Multiple comparisons of *p* values (2-tailed); *Ra* [µm] (DATA) Independent (grouping) variable: f_{rev} [mm·rev^{-1}] Kruskal-Wallis test: H(2, N=16) =12.72459 *p*=0.0017		
	0.4 mm·rev^{-1} R:4.5000	0.6 mm·rev^{-1} R:10.500	1.0 mm·rev^{-1} R:14.500
0.4 mm·rev^{-1}	-	0.118775	0.001811
0.6 mm·rev^{-1}	0.118775	-	0.704291
1.0 mm·rev^{-1}	0.001811	0.704291	-

The third independently examined variable factor was the cutting depth a_P. It is affected by 16.32 % in the case of a change in the investigated *Ra* response. The influence of the cutting depth on the surface roughness results from changes in the deformation processes in the cutting zone when changing the depth of cut. The literature sources document a negligible influence of the cutting depth on the roughness of the surface. By increasing the cutting depth, the roughness will decrease slightly if the cutting rate and feed rate are constant.

3.2. Results and discussion for parameter Rz

Similarly, as for the investigated parameter *Ra*, it is also possible for the investigated parameter *Rz* to analyse the assumed dependences and to express the model (3)

$$Rz = const \cdot v_c^{x_1} \cdot f_{rev}^{x_2} \cdot a_P^{x_3} \qquad (3)$$

An Analysis of the investigated parameter *Rz* shows that the model (3) under a constant action of the tool RNGN43-LX11-TUNGALOY represents 97.22 % of the variability of the investigated parameter Rz at the changes of the cutting conditions. This conclusion can be accepted on the basis of the value of the adjusted index of determination. The average value *Rz* = 10.546 µm and estimate of the standard deviation of random error are 0.83876. The chosen mathematical and statistical dependence according to the Cohen scale can, therefore, be considered functional. The analysis of the model (3) using the Fisher's analysis of variance points to the fact that from the total variability of the model with 15 degrees of freedom and the sum of squares of deviations of 1.0729, only 0.02389 of the sum of squares of deviations represent errors, which is 2.23 %. The remaining almost 98 % of the total variability belongs to the model. On the basis of the achieved level of significance of the Fisher-Snedecor test criterion (*p* = 0.0001), it can be concluded that the model (3) contains at least one effect that significantly affects the

change in the *Rz* value. Therefore, at the chosen level of significance, the model (3) can be considered adequate. On the basis of the above analysis, it is possible to obtain individual coefficients of equation (3) using the least squares method with the identification of their statistical significance.

[Table 9 about here.]

Table 9 Estimates of the parameter of the investigated dependence for the variable *Rz*.

Term	Estimate	Std Error	t Ratio	Prob>|t|	Lower 95 %	Upper 95 %
const	-0.9965750	0.492307	-2.02	0.0658	-2.069220	0.076070
x_1	0.2392116	0.142229	1.68	0.1184	-0.070680	0.549102
x_2	2.5029316	0.179188	13.97	<0.0001*	2.112515	2.893348
x_3	-2.2118640	0.351458	-6.29	<0.0001*	-2.977630	-1.446100

It follows from Table 9 that a statistically significant factor influencing the change of the investigated response *Rz* is primarily the feed rate, with a 58.305 % influence on its change, as well as the cutting depth that contributes to a change in *Rz* variability of 26.252 %. For the parameter *Rz*, at the level of significance of α = 5 %, no significant influence of the cutting rate and an absolute element, or of the model constant (3) was proven. Precisely the statistical insignificance of the constant indicates that within the realised experiment only important input factors were used. By substituting the coefficients from Table 9 to the model (3), we obtain the final form of the statistical prediction function of the dependence of the value of the investigated response *Rz* on the cutting conditions for the feed turning of the coating Stellite 6 with the use of the tool RNGN43 LX11-TUNGALOY (4). These conclusions are also confirmed by simulation of experimentally obtained results using the neural network. At the nodes of a neural network, analogously called neurons, each input variable xi at the input of the jth neuron is multiplied by the weighting factor wji. The sum $z_j = w_{0j} + \Sigma w_{ji} \cdot x_i$ is in a neuron transformed by the activation function. The activation function expresses the intensity of the neuron response to the given input. The most commonly used activation functions include the logistic function, $\sigma_j(z)$=1/(1+e-z), which resembles the biological sensoric response function. The weights wji represent the intensity of the linkage between the variable and the neuron, or, in the case of multilayer networks, between the neurons in the layers. These linkages are sometimes called synapses. The output variables are predicted as weighted linear combinations of outputs from the last hidden neuron layer. Thus, the neural network is formally a special case of multiple nonlinear regression; the neural network can be virtually considered to be a nonparametric regression. If the neural network contains no hidden layer of neurons, only the input and output variables, it would be a linear regression model. The neural network is optimised using the smallest square criterion. This means that the network is set in a way that the sum of squares of the predicted and measured value of the output variable is minimal. This setting is the objective of an iterative optimisation procedure, called learning or training of a neural network. The optimisation procedure uses adaptive Gauss-Newton algorithms. For the application of the neural network, the

experimentally obtained response values *Rz* were divided by a ratio of 85 % to 15 %, the first group being used as data for learning and the second group as data for testing. The basic used neural network with three layers (the first containing 3 neurons and the other two hidden layers contained 2 neurons each) reached a maximum error for learning data value of 0.004346201313 and a mean error for learning data value of 0.0009920144294. The maximum error for the tested data is 0.003247050035 and the mean error is 0.001291113035. These values, along with the graphical representation of the learning process (Figure 4), demonstrate good quality of the model and they express both the improvement of the model and the improvement of the prediction of valid data. The model in question therefore predicts well from unknown data, and at the same time, it predicts both curves, i.e. both for learning data and for testing data.

[Fig. 4 about here.]

From the analysis of the model generated by the neural network, the residues represent 12.026 from the total sum of the deviations squares of 768.408, which is 1.57 %. The remaining 98.44 % represents an explanation of the sum of squares by the model. The achieved level of significance of the Fisher test criterion reaches the value p = 0.00417, which means that at the significance level α = 5 % the model can be considered to be significant. From the viewpoint of the relative influence of the predictors on the change in the value of the monitored response *Rz* (Figure 5), it can be concluded that it is namely the feed rate, which has the dominant influence. The cutting depth also contributes significantly to the change in the value of the *Rz* parameter and, as in previous analyses, the influence of the cutting speed was only minimal.

The influence of the feed rate (Figures 5 and 6) on the change of the *Rz* (4) value is connected not only with the geometric causes of formation of the resulting surface micro-geometry, but it also considerably influences the elastic and plastic deformations in the surface layer.

$$R_Z = 0.101 \cdot v_c^{0.239} \cdot f_{rev}^{2.503} \cdot a_p^{2.212} \qquad (4)$$

[Fig. 5 about here.]

[Fig. 6 about here.]

The influence of the feed rate on the change of the *Rz* value has to be also observed in relation to the cutting rate. If we increase the feed rate from 0.4 mm·rev^{-1} to 0.6 mm·rev^{-1} at a constant cutting rate and constant cutting depth, the value of the parameter *Rz* will increase by 175.90 %, i.e. from the value of 5.5 μm to the value of 15.175 μm. If at a constant cutting rate and a constant cutting depth we increase the feed rate from the value of 0.6 mm·rev^{-1} to 1.0 mm·rev^{-1}, the value of the *Rz* parameter will increase already by 259.16 %. It means therefore that at maintained constant cutting conditions (cutting rate, cutting depth), when the feed rate increases from 0.4 mm·rev-1 to 0.5 mm·rev^{-1}, then the value of the roughness parameter *Rz* will increase by 74.81 %. This increase in roughness value *Rz* decreases with an

increasing feed rate. The average value of the change in the roughness *Rz* at an increase in feed rate by 0.1 mm·rev^{-1} represents the value of 47.312 mm·rev^{-1}.

When observing the change in the *Rz* value in dependence on the change in feed rate with simultaneous change in the cutting rate (Figure 7), it can be observed that by increasing the cutting rate, the *Rz* value increases with the increased feed rate, while the change in the *Rz* value caused by the cutting rate is small. It varies from 2.55 % to 3.75 % with an increase of the cutting rate from 150 m·min^{-1} to 250 m·min^{-1} in increments of 25 m·min^{-1}. The cutting depth has a more significant influence on the change of the *Rz* value. An increase of the cutting depth from 0.1 mm to 0.15 mm reduces the *Rz* value by approx. 59 %. However, this reduction in the given cutting depth interval must be attributed to the machined material as such. When increasing the cutting depth by more than 0.15 mm, it is possible to expect on the contrary a deterioration of the roughness *Rz.*

[Fig. 7 about here.]

4 Conclusion

Based on detailed research, a new contribution of stellite 6 alloy machining technology has been established to create new prediction equations of variation of surface roughness *Ra*, *Rz* on cutting speed, feed and cutting depth (2), (4). From experimental results in the range of cutting rates from 150 to 250 m·min^{-1}, feed rates from 0.4 to 1.0 mm·rev^{-1} and cutting depths of 0.1 and 0.15 mm, the predictive models of roughness parameters *Ra* and *Rz* were compiled using mathematical and statistical methods followed by subsequent application of neural networks in order to confirm the obtained conclusions. The surface roughness parameters were measured with the use of a contact profile meter. The experimental results have demonstrated that feed turning technology was a suitable technology for machining coatings created by thermal spraying of Stellite 6 alloy in such user cases where additional surface treatment is required for specific reasons, and it is appropriate. In the use and exploitation of coatings applied by thermal spraying, the surface of the formed coatings or the machining of this surface plays a major role. From a practical viewpoint, if it is not absolutely necessary to process the coating, it is often preferable to leave the surface in the as-sprayed condition. Several good and well-founded reasons support this simpler procedure:

- What concerns the adhesion of coatings, the component of mechanical anchoring of these coatings to the surface of the background material plays a significant role. Any interference with the surface of a relatively thin coating may significantly contribute to the failure or at least to disturbance of the mechanical anchoring.
- Each mechanical treatment of the surface leads to the introduction of stress into the coating, and in any case, it leads to rearrangement of the already existing stress in the coating.
- Coatings applied by thermal spraying consist in principle of individual deformed particles of the additive material deposited on each other, in any case with a certain amount of porosity. During mechanical treatment of such a coating composition, it is necessary to take into account that the

contact tool-coating is characterised by an intermittent cutting, which results in further adverse consequences consisting of a shock effect on the coating.

- As a result of oxidation and other physical-chemical processes, the coatings are mostly composed of very hard and brittle phases, which in themselves bring considerable difficulties during their mechanical treatment.
- Mechanical treatment of applied coatings results in a loss of one of the significant advantages of thermal-spraying, which is the formation of thin coatings at certain parts of the surface of components or parts, without any subsequent mechanical treatment of the coatings, thus saving labour and often also deficient and economically expensive coating material.

For further study of the technological possibilities of turning of hot sprays, attention should be paid, in addition to the influence of cutting conditions, to the appropriate geometry of the cutting wedge and to the cutting forces, which are formed in the process, as they often play a key role in relation to the mechanical properties of the spray application. Because the structure of the applied coating is composed of deformed particles of the additive material, the surface roughness of the applied coatings is greatly influenced by the granularity and grain size composition of the additive material. Generally speaking, the larger the particle of the deposited material, the greater is the surface roughness of the applied coating. The good message is that the roughness after spraying is mostly sufficient for the functional use of coatings. This fact has led the producers of the additive materials to the idea of producing additive materials with different grain sizes ranging from coarse to very fine ones. Of all the methods of mechanical treatment of coatings applied by thermal spraying, the grinding became the most used, and in the case of ceramic coatings, the grinding with the use of diamond tool became the most used. The grinding requires in all cases an intensive cooling. Poor cooling, or even no cooling, leads to the formation of a mesh of surface cracks in coatings, especially in ceramic coatings. The efforts to achieve the maximum economic effect of mechanical machining of applied coatings lead to the verification of the possibilities of machining of these coatings by turning. At present, turning can be used only for machining of the coatings applied by thermal spraying having relatively good plastic properties and relatively low hardness. This type of turning commonly uses higher cutting rates and small feed rates. However, a big problem exists with the use of turning in the case of an intermittent cutting. The allowances required for mechanical machining of the coating, and thus the required thickness of the coating, are also governed by the surface roughness in the state after spraying, and it can be said that they are dependent also on the technological method of the thermal spraying.

Declarations

Acknowledgement: The present contribution has been prepared under project LO1502 ‘Development of the Regional Technological Institute‘ under the auspices of the National Sustainability Programme I of the Ministry of Education of the Czech Republic aimed to support research, experimental development and innovation.

Conflict of interest

The author(s) declared no potential conflicts of interest with respect to the research, authorship, and/or publication of this article.

Authors' contribution

J.Ř. and M.G wrote the paper, J.V., M.K. and M.H. analyzed the data, J. F., Š. H – Š. and A.V performed experiments.

Declaration of interests

The authors declare that they have no known competing financial interests or personal relationships that could have appeared to influence the work reported in this paper.

References

1. Aykut Ş, Gölcü M, Semiz S, Ergür HS (2007) Modeling of cutting forces as function of cutting parameters for face milling of satellite 6 using an artificial neural network. J Mater Process Technol 190:199–203
2. Agarwal SC, Ocken H (1990) The microstructure and galling wear of a laser-melted cobalt-base hardfacing alloy. Wear 140:223–233
3. Aykut Ş, Bagci E, Kentli A, Yazıcıoğlu O (2007) Experimental observation of tool wear, cutting forces and chip morphology in face milling of cobalt based super-alloy with physical vapour deposition coated and uncoated tool. Mater Des 28:1880–1888
4. Shokrani A, Dhokia V, Newman ST (2012) Environmentally conscious machining of difficult-to-machine materials with regard to cutting fluids. Int J Mach Tools Manuf 57:83–101
5. Monroy K, Delgado J, Ciurana J (2013) Study of the pore formation on CoCrMo alloys by selective laser melting manufacturing process. Procedia Eng 63:361–369
6. Marek I, Novák P, Mlynár J, Vojtěch D, Kubatík TF, Málek J (2015) Powder metallurgy preparation of Co-based alloys for biomedical applications. Acta Phys Pol A 128:597–601
7. Salahshoor M, Guo YB (2011) Cutting mechanics in high speed dry machining of biomedical magnesium - calcium alloy using internal state variable plasticity model. Int J Mach Tools Manuf 51:579–590
8. Sahin O, Tuncdemir R, Cetinkara HA, Guder HS, Sahin E (2011) Production and mechanical behaviour of biomedical CoCrMo alloy. Chin Phys Lett 28:126–201
9. Sánchez-De Jesús F, Bolarín-Miró M, Torres-Villaseñor G, Cortés-Escobedo C, Betancourt-Cantera J (2010) Mechanical alloying of biocompatible Co-28Cr-6Mo alloy. J Mater Sci Mater Med 21:2021–2026
10. Fang L, Yan H, Yao Y, Zhang P, Gao Q, Qin Y (2018) Reactive fabrication and effect of NbC on microstructure and tribological properties of CrS Co-based self-lubricating coatings by laser cladding. Materials 11:44

11. Milošev I (2012) CoCrMo Alloy for Biomedical Applications. In: Djokić SS (ed) Biomedical Applications. Modern Aspects of Electrochemistry. Springer, Boston, MA, pp 1–72
12. Niinomi M (2002) Recent metallic materials for biomedical applications. Metall Mater Trans A 33A:477–486
13. Podgornik B, Vižintin J, Wänstrand O, Larsson M, Hogmark S, Ronkainen H, Holmberg K (2001) Tribological properties of plasma nitrided and hard coated AISI 4140 steel. Wear 249:254–259
14. Yang Q, Mckellar R (2015) Nanolayered CrAlTiN and multilayered CrAlTiN–AlTiN coatings for solid particle erosion protection. Tribol Int 83:12–20
15. Bewilogua K, Bräuer G, Dietz A, Gäbler J, Goch G, Karpuschewski B, Szyszka B (2009) Surface technology for automotive engineering. CIRP Ann Manuf Technol 58:608–627
16. Sohi MH, Ghadami F (2010) Comparative tribological study of air plasma sprayed WC–12% Co coating versus conventional hard chromium electrodeposit. Tribol Int 43:882–886
17. Wood RJK (2010) Tribology of thermal sprayed WC–Co coatings. Int J Refract Metals Hard Mater 28:82–94
18. Weinert K, Inasaki I, Sutherland JW, Wakabayashi T (2004) Dry machining and minimum quantity lubrication. CIRP Ann Manuf Technol 53:511–537
19. Shao H, Li L, Liu LJ, Zhang SZ (2013) Study on machinability of a stellite alloy with uncoated and coated carbide tools in turning. J Manuf Process 15:673–681
20. dos Santos Cabral T, Dias SE, Castro Filho AA, Baia PEC, Borges DJA, de Magalhães Braga E (2018) Influence of a cobalt-based wire injection in austenitic coating deposited via CW-GMAW. J Braz Soc Mech Sci & Eng 40:461
21. Jawahir IS, Brinksmeier E, M'Saoubi R, Aspinwall DK, Outeiro JC, Meyer D, Umbrello D, Jayal AD (2011) Surface integrity in material removal processes: Recent advances. CIRP Ann Manuf Technol 60:603–626
22. Sun S, Brandt M, Dargusch MS (2010) Thermally enhanced machining of hard-to-machine materials-A review. Int J Mach Tool Manu 50:663–680
23. Chinchanikar S, Choudhury SK (2013) Effect of work material hardness and cutting parameters on performance of coated carbide tool when turning hardened steel: An optimization approach. Measurement 46:1572–1584
24. Berger LM (2015) Application of hardmetals as thermal spraying coatings. Int J Refract Metals Hard Mater 49:350–364
25. López de Lacalle LN, Gutiérrez A, Lamikiz A, Fernandes MH, Sánchez JA (2001) Turning of thick thermal spray coatings. J Therm Spray Technol 10:249–254
26. Klimenko SA, Mel'niichuk YA, Vstovskii GV (2008) Interrelation between the structure parameters, mechanical properties of sprayed materials and the tool life in cutting them. J Superhard Mater 30:115–121

27. Carou D, Řehoř J, Vilček I, Houdková-Šimůnková Å (2015) An approach to the machining of hard coatings prepared by laser cladding and thermal spraying. Strojírenská technologie – Plzeň. University of West Bohemia, Pilsner, pp 47–53
28. Rubio EM, Villeta M, Saá AJ, Carou D (2012) Analysis of main optimization techniques in predicting surface roughness in metal cutting processes. Appl Mech Mater 217:2171–2182
29. Ancio F, Gámez AJ, Marcos M (2015) Factors influencing the generation of a machined surface. Application to turned pieces. J Mater Process Technol 215:50–61
30. Suresh R, Basavarajappa S, Gaitonde VN, Samuel GL (2012) Machinability investigations on hardened AISI 4340 steel using coated carbide insert. Int J Refract Metals Hard Mater 33:75–86
31. Belmonte F, Oliveira FJ, Sacramento J, Fernandes AJS, Silva RF (2004) Cutting forces evolution with tool wear in sintered hardmetal turning with CVD diamond. Diam Relat Mater 13:843–847
32. Almeida FA, Oliveira FJ, Sousa M, Fernandes AJS, Sacramento J, Silva RF (2005) Machining hardmetal with CVD diamond direct coated ceramic tools: effect of tool edge geometry. Diam Relat Mater 14:651–656
33. Ozturk S (2014) Machinability of Stellite-6 coatings with ceramic inserts and tungsten carbide tools. Arab J Sci Eng 39:7375–7383
34. Houdková Å, Pala Z, Smazalová E, Vostřák M, Česánek Z (2017) Microstructure and sliding wear properties of HVOF sprayed, laser remelted and laser clad Stellite 6 coatings. Surf Coat Techno 318:129–141
35. Houdková Å, Smazalová E, Pala Z (2016) Effect of Heat Treatment on the Microstructure and Properties of HVOF-Sprayed Co-Cr-W Coating. J Therm Spray Technol 25:546–557
36. Valíček J, Řehoř J, Harničárová M, Gombár M, Kušnerová M, Fulemová J, Vagaská A (2019) Investigation of Surface Roughness and Predictive Modelling of Machining Stellite 6. Materials 12:2551

Figures

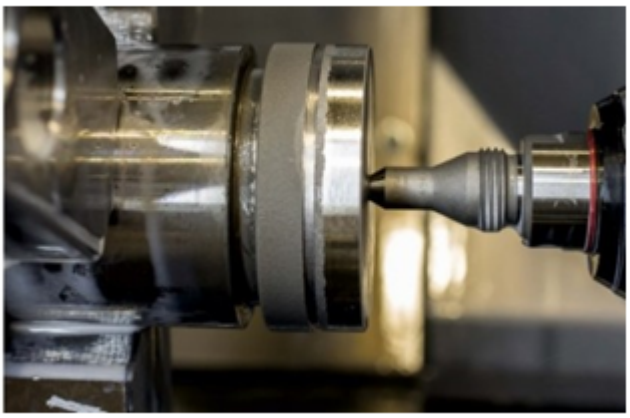

Figure 1

Views on experimental verification (experiment 1).

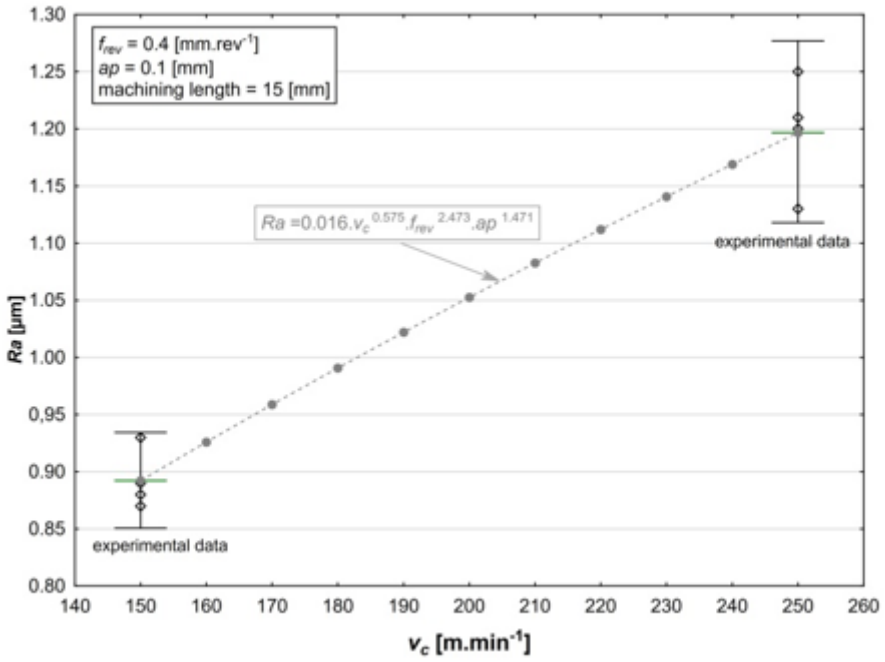

Figure 2

Dependence of the change of the surface roughness *Ra* on the cutting rate v_c.

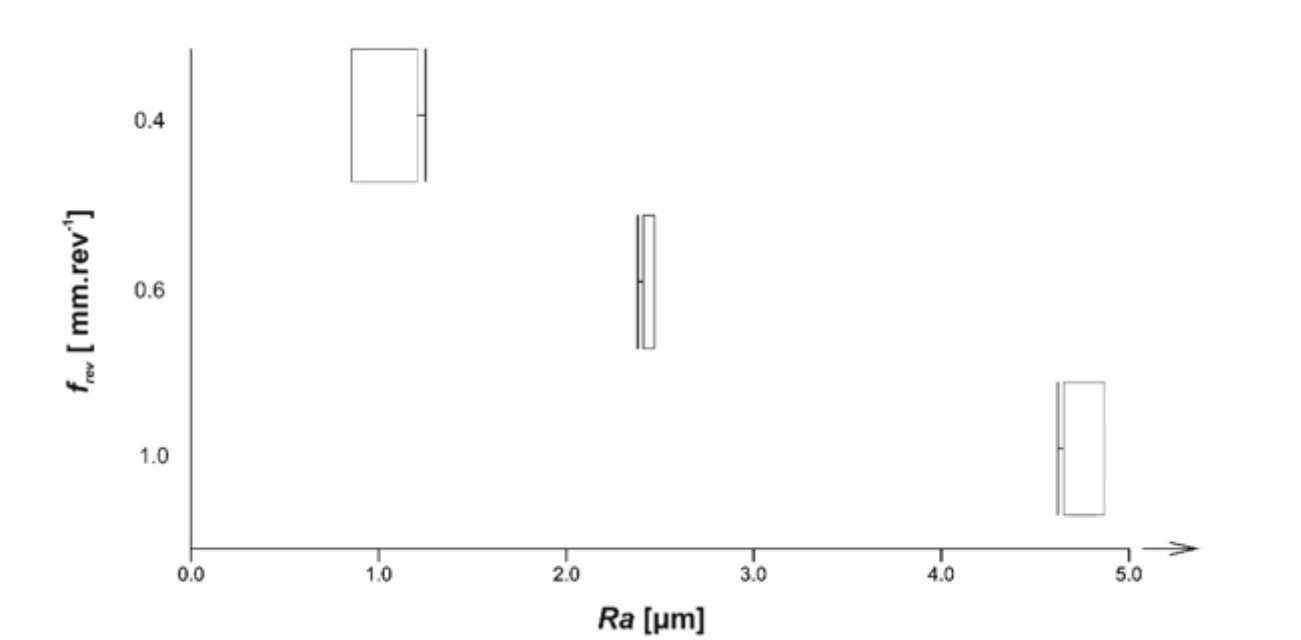

Figure 3

Dependence of change of the value of surface roughness *Ra* on the feed rate f_{rev}.

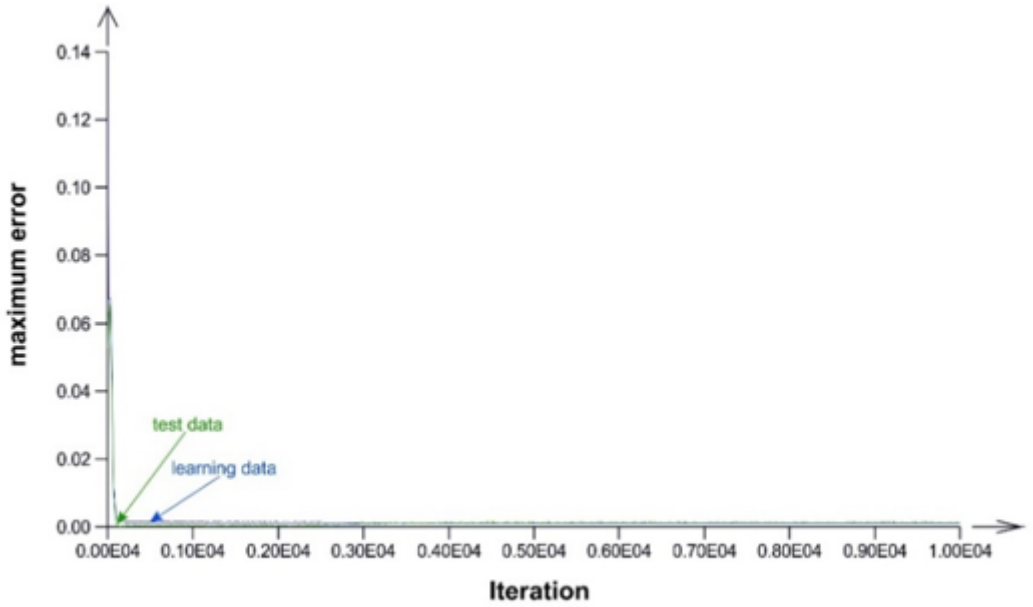

Figure 4

Diagram of the learning process for the response *Rz*.

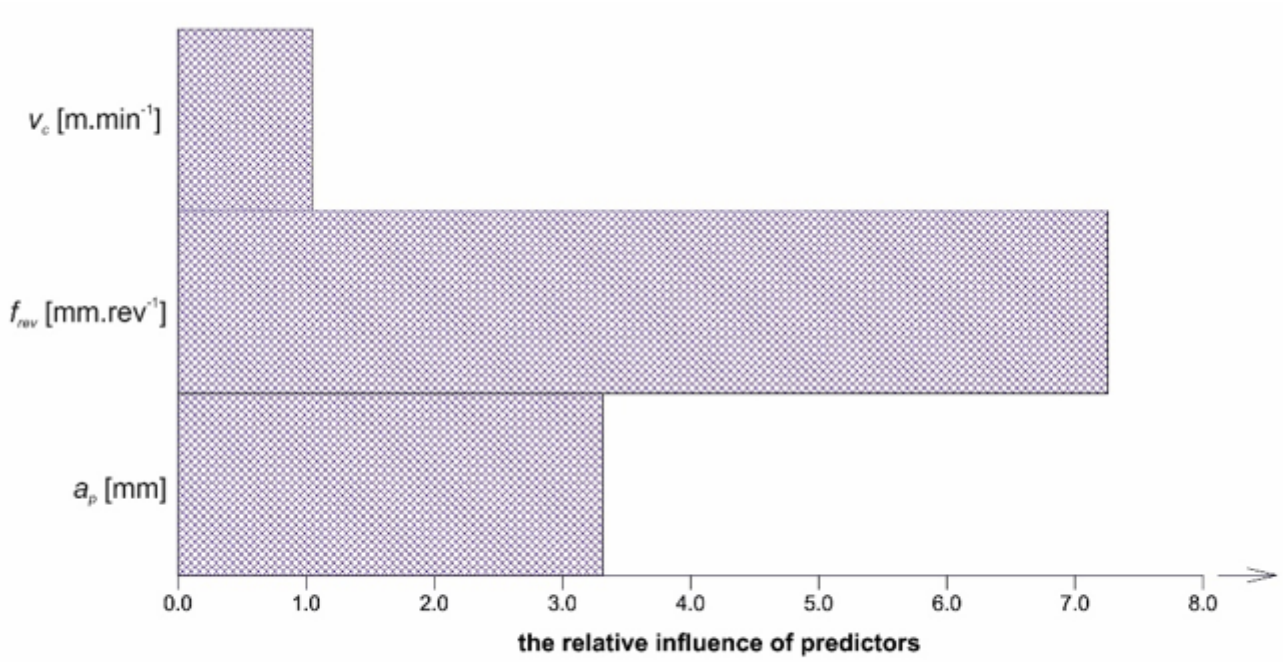

Figure 5

Relative influence of predictors on change of the value *Rz*.

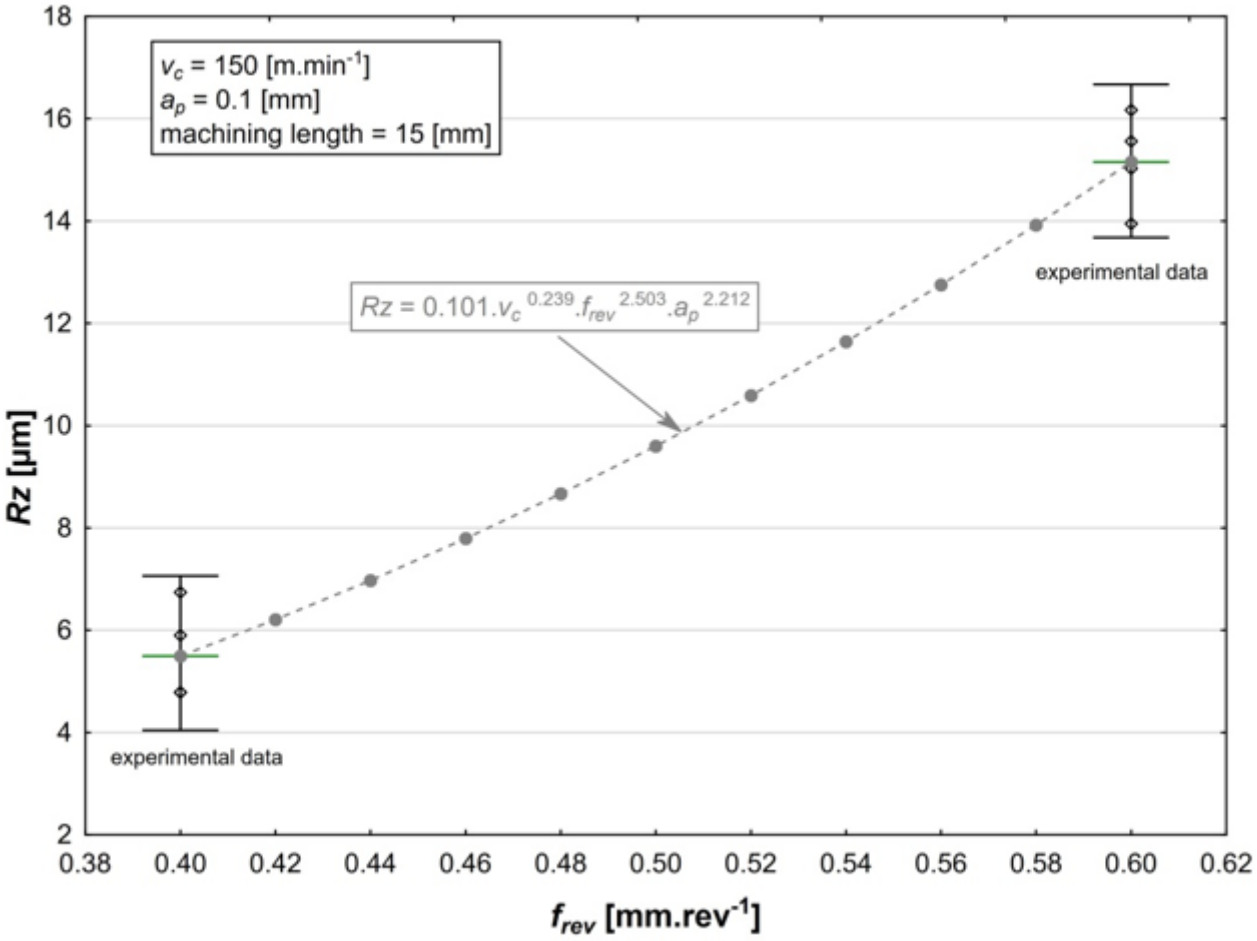

Figure 6

Influence of the change of the *Rz* value on the feed rate.

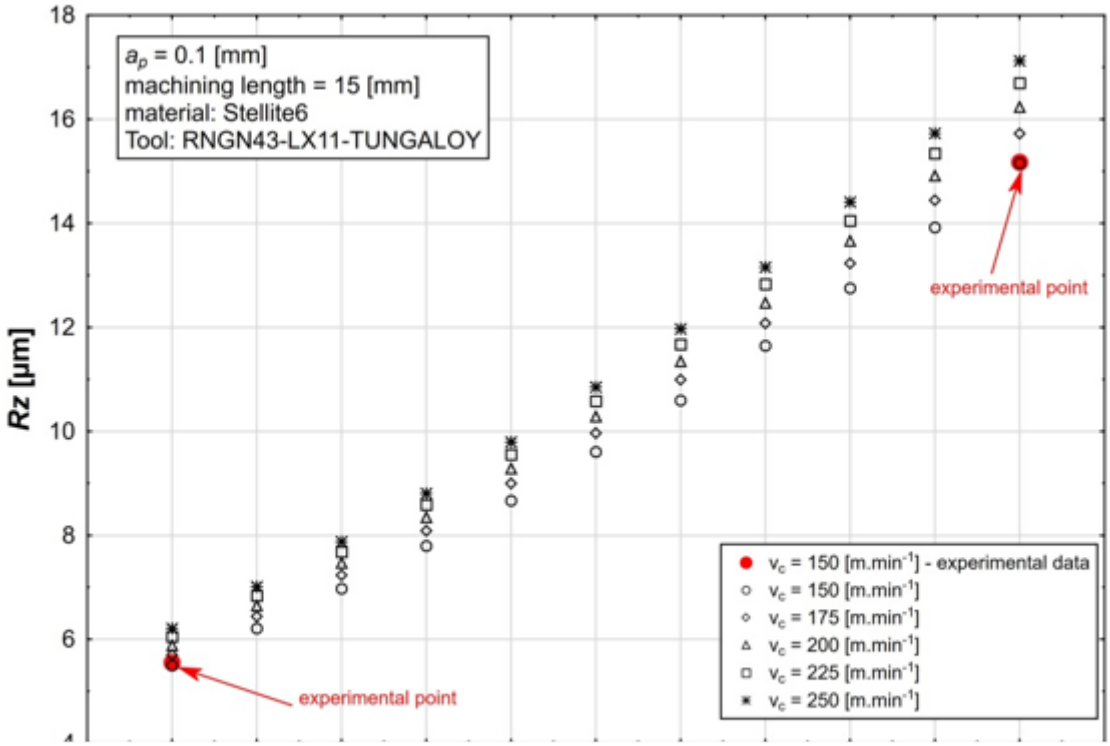

Figure 7

Dependence of the change in the value *Rz* on the feed rate with simultaneous change of the cutting rate.